analytical chemistry

Article

Cite This: *Anal. Chem.* 2019, 91, 12000−12005

pubs.acs.org/ac

Bidirectional Electrochemiluminescent Sensing: An Application in Detecting miRNA-141

Zhi-Hong Xu, Hui Wang, Jing Wang, Wei Zhao,* Jing-Juan Xu,* and Hong-Yuan Chen

State Key Laboratory of Analytical Chemistry for Life Science, School of Chemistry and Chemical Engineering, Nanjing University, Nanjing 210023, China

Supporting Information

ABSTRACT: This paper describes a bidirectional electrochemiluminescence (ECL) biosensor for the detection of microRNA-141 (miRNA-141) with aM level detection limit and two-segment 8 orders of magnitude linear range. Hemin/G-quadruplex DNAzyme was assembled on carbon nitride nanosheets and Au nanoparticles modified electrode. The ECL of carbon nitride nanosheets could be enhanced by the right amount of H_2O_2 (no more than 10 mM) and then inhibited by excessive H_2O_2 when 0.1 M $K_2S_2O_8$ acted as coreactant. In the presence of excessive H_2O_2 (20 mM), a recovery of ECL intensity was obtained due to the catalytic reduction of H_2O_2 caused by hemin/G-quadruplex DNAzyme at lower target concentrations, and then an ECL decrease occurred mainly by biocatalytic precipitation (BCP)-induced charge transfer resistance on the electrode surface at higher target concentrations. Therefore, based on the change of the ECL intensity caused by the catalytic reduction of H_2O_2 and BCP, a highly sensitive bidirectional miRNA sensor with ultralow detection limit of 7.9 aM and wide linear range from 10^{-17} to 10^{-9} M was obtained. This work could attract more attention on the study of multiple mechanisms and also provides a more sensitive and precise method for the analysis of nucleic acids.

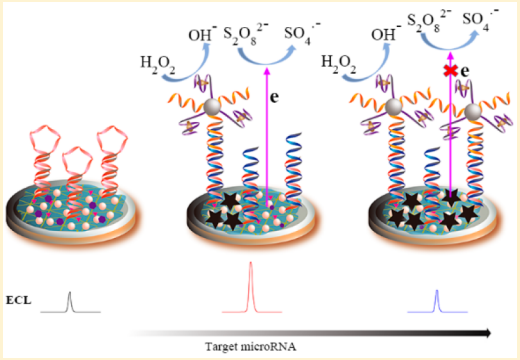

MicroRNAs (MiRNAs), as a class of noncoding molecules with 18−25 nucleotides, are closely associated with a variety of human cancers.[1,2] Latest studies shows that miRNAs released from cancer cells could be present in human plasma in stable form, named circulating miRNAs, which become new biomarkers in early tumor diagnosis. However, as miRNAs show ultralow abundance (<1.0 pM) in normal human serum and hugely fluctuate as the disease progresses, it is highly desirable to develop ultrasensitive sensing strategy with wide detection range. Up to now, more and more methods were developed for the detection of miRNAs,[3] such as differential pulse voltammetry (DPV),[4] surface plasmon resonance (SPR),[5] fluorescence,[6] and electrochemiluminescence (ECL).[7]

ECL is a process in which sequential electron-transfer reactions on the surface of the electrode induce luminescence.[8] As an electrochemical technique, ECL shows outstanding features including high sensitivity, ease of operation, and spatiotemporal controllability.[9−12] In order to obtain better performance, ECL was used in the applications combined with other techniques.[13] For example, Aflatoxin B1 (AFB1) was detected by the combination of ECL and square-wave voltammetry (SMV), which resulted in accurate and sensitive analytical performance for AFB1 with good linear range and detection limit.[14] In addition, the study of Zhang group took advantage of the ECL and electrochemical impedance spectroscopy (EIS) to explain the competition of catalytic reaction and steric hindrance effect on the surface of the electrode in biosensing system, resulting in high sensitivity and wide detection range for the detection of 8-hydroxy-2′-deoxyguanosine.[15]

In this work, we reported a bidirectional ECL biosensor based on the competition between catalytic reaction and steric hindrance effect induced by biocatalytic precipitation (BCP) for the analysis of microRNA-141. As shown in Scheme 1, a composite of C_3N_4 nanosheets and Au nanoparticles (C_3N_4−AuNPs), which exhibited excellent catalytic, optical, and electronic advantages, was applied as the luminophore for ECL sensing.[16] Target miRNA-141 triggered the start of an improved catalytic hairpin assembly (CHA) process, following by the assembly of hemin/G-quadruplex DNAzyme-microbeads (MBs), which served as catalysts for both biocatalytic precipitation (BCP) and electrochemical reduction of H_2O_2. The ECL of C_3N_4 was initially inhibited by excessive H_2O_2, while catalytic decomposition of H_2O_2 by the assembled DNAzyme retrieved the ECL response. On the other hand, the increased amount of DNAzyme-stimulated BCP layer inhibited the electron transfer at the surface of the electrode, which resulted in enhanced impedance and reduced ECL signal. Based on the competition between catalytic effect and steric hindrance effect, miRNA-141 could be quantified with a

Received: June 27, 2019
Accepted: August 14, 2019
Published: August 14, 2019

DOI: 10.1021/acs.analchem.9b02914
Anal. Chem. 2019, 91, 12000−12005

Scheme 1. Schematic Illustration of the Bidirectional ECL Biosensor for miRNA-141

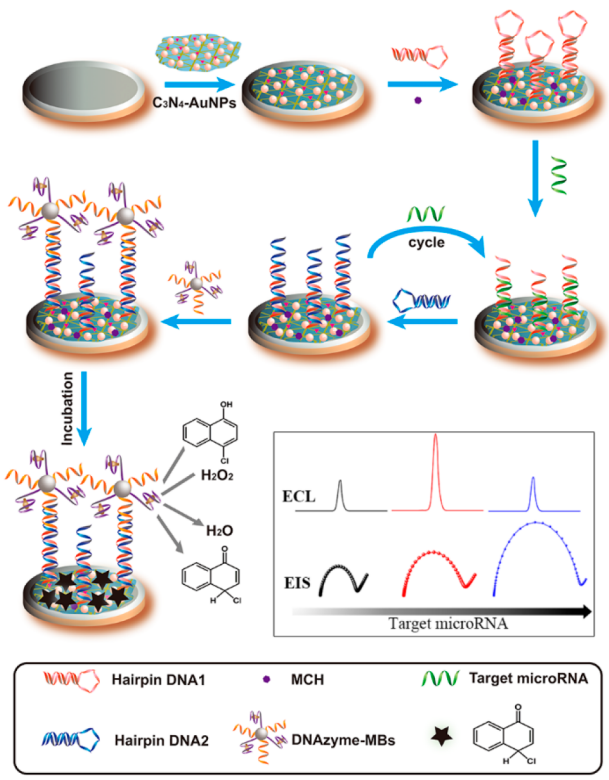

detection limit of 7.9 aM (S/N = 3) and wide linear range of 8 orders of magnitude.

EXPERIMENTAL SECTION

Reagents and Apparatus. Apparatus and reagents used in this research are displayed in the Supporting Information. DNA and miRNA sequences are shown in Table S1

Synthesis of C_3N_4–AuNPs. The C_3N_4 material was purchased from Nanjing XFNANO Materials Tech Co., Ltd. C_3N_4–AuNPs were synthesized according to related references.[17−19] In general, 90 μL of 0.01 M $HAuCl_4$ solution was injected into C_3N_4 suspension (0.1 mg/mL) under stirring. The mixed solution was ultrasonicated for 10 min, followed by stirring for 2 h at normal temperature. These two steps were repeated for another two times again. Afterward, 225 μL of 0.01 M fresh $NaBH_4$ solution was added quickly to the mixture in an ice bath, followed by stirring for 20 min. Next, 90 μL of 0.01 M sodium citrate solution was added dropwise to the reaction mixture and then kept stirring for 0.5 h at normal temperature. The final nanohybrid material was centrifuged at 8000 rpm for 5 min, and the precipitate was washed by ultrapure water after removing the supernatant. Centrifugation and washing procedures were repeated in sequence three times in order to get rid of redundant Au NPs, unreacted $NaBH_4$, and sodium citrate. In the end, the precipitate was redispersed in 8 mL of ultrapure water and stored at 4 °C for further use.

Preparation of Modified Magnetic Beads. In order to obtain the activated magnetic beads, 10 mM EDC and 20 mM NHS were used to react with carboxyl-modified magnetic bead suspension (5 mg/mL) at 37 °C for 1 h. Afterward, capture DNA and G-quadruplex were added into the activated magnetic beads suspension and reacted for 12 h to obtain the DNA magnetic beads. Two weight percent BSA was used to block the nonspecific active binding sites of the DNA magnetic beads after being washed with PBS buffer. Thus, the solution of bioconjugates was dispersed into 0.2 mM hemin, which was dissolved in a buffer solution containing 1% DMSO,

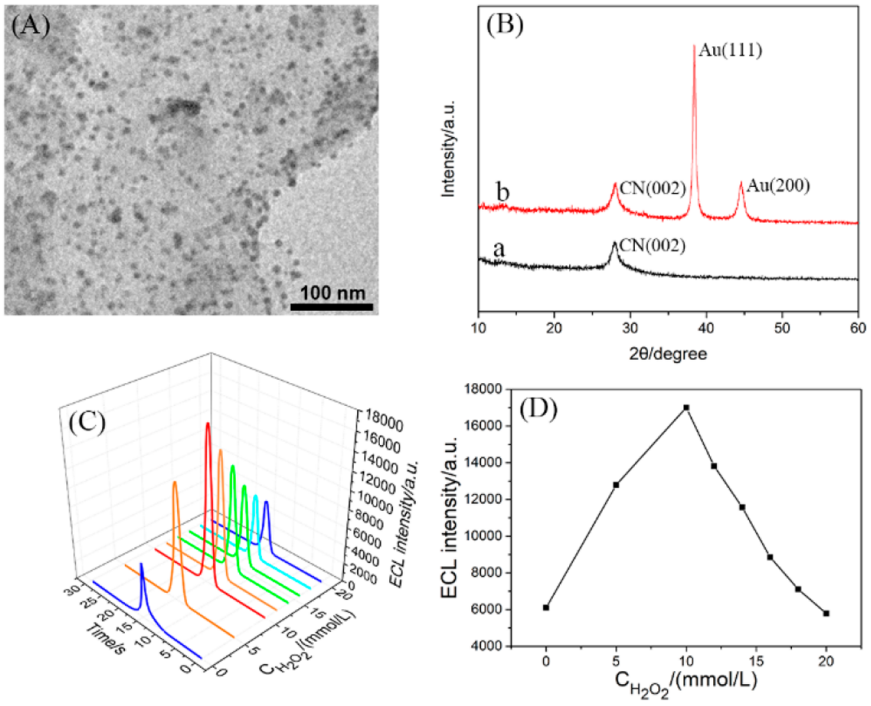

Figure 1. (A) TEM image of C_3N_4–AuNPs. Voltage: 100 kV. Magnification: 80k. (B) XRD patterns of (a) C_3N_4 and (b) C_3N_4–AuNPs. (C) and (D) ECL responses of C_3N_4–AuNPs with H_2O_2 of different concentrations in 0.01 M PBS (pH 7.4) containing 0.1 M $K_2S_2O_8$.

DOI: 10.1021/acs.analchem.9b02914
Anal. Chem. 2019, 91, 12000−12005

0.05% Triton X-100, 25 mM HEPES, 20 mM KCl, and 200 mM NaCl and then incubated for 1 h to form DNAzyme-MBs.

Fabrication of the ECL Biosensor. The assembly of ECL biosensor is displayed in Scheme 1. As a substrate for immobilizing C_3N_4–AuNPs, the glassy carbon electrode (GCE) was polished with alumina slurry and ultrasonicated in the ultrapure water and ethanol in sequence. First, 10 μL of C_3N_4–AuNPs solution was dropped onto the surface of GCE and dried in air to obtain C_3N_4–AuNPs film modified GCE. Then the GCE/C_3N_4–AuNPs was incubated with 100 μL of the solution of Hairpin DNA 1 (H1) (1.0×10^{-6} M) overnight at 4 °C, which was processed by 10 mM TCEP to cut off the S–S bond before use. Subsequently, the acquired electrode was blocked by MCH (100 μM) for 1 h at room temperature. Then, the gaining electrode was incubated with 100 μL of miRNA-141 with different concentrations at 37 °C for 2 h. After being washed with PBS buffer, the resulting electrode was incubated with 100 μL of 1.0×10^{-6} M Hairpin DNA 2 (H2) at 37 °C for 2 h to replace miRNA-141. Finally, the modified electrode was immersed into the solution of DNAzyme-MBs mentioned above for further hybridization. 4-CN was dissolved in ethanol and then diluted with 0.1 M PBS buffer, and the final solution was composed of 1.0×10^{-3} M 4-CN and 2% (v/v) ethanol. Then the DNAzyme-MBs-modified GCE was immersed in the BCP solution composed of 1.0×10^{-3} M 4-CN and 1.0×10^{-6} M H_2O_2 for 30 min and rinsed with PBS for ECL measurement. The successful assembly of each step for the sensing system was characterized by EIS (Figure S1). ECL measurement was conducted by immersing the electrodes in 0.01 M PBS (pH 7.4) containing 0.1 M $K_2S_2O_8$ and 20 mM H_2O_2 and scanned from 0 to −1.5 V. EIS detection was accomplished with the electrodes in the solution containing 0.1 M KCl, 5 mM $K_3[Fe(CN)_6]$, and $K_4[Fe(CN)_6]$.

RESULT AND DISCUSSION

Characterization of C_3N_4–AuNPs. Au NPs were introduced onto the C_3N_4 in order to enhance the conductivity of C_3N_4 and provide bonding sites for thiol-modified H1. Figure 1A shows the TEM image of the hybridized C_3N_4–AuNPs. A large amount of Au NPs were distributed on the surface of C_3N_4. Figure 1B shows the XRD patterns of C_3N_4 and C_3N_4–AuNPs. The characteristic diffraction peak of C_3N_4 is observed at 27.8°, which can be assigned to the (002) graphitic interlayer structure. After the deposition of AuNPs, the typical diffraction peaks of Au at 38.4° (111) and 44.6° (200) can be unambiguously labeled in the XRD pattern of C_3N_4–AuNPs, indicating the successful attachment of AuNPs on the C_3N_4.[15,20] Besides the TEM image of C_3N_4, UV–vis absorption spectra of C_3N_4 and C_3N_4–AuNPs are displayed in Figure S2. Figure S3 demonstrates great ECL stability for C_3N_4–AuNPs.

The previous study of our group indicated that the ECL intensity of semiconductor TiO_2 nanotubes (NTs) and CdS nanocrystal film would enhance initially and then decrease with the increasing concentration of H_2O_2 when $K_2S_2O_8$ served as coreactant.[21] The reason for this phenomenon was considered to be that a small quantity of $OH^\bullet$ would promote the formation of $SO_4^{\bullet-}$ and excessive $OH^\bullet$ would scavenge the $SO_4^{\bullet-}$. In this work, the ECL intensity of C_3N_4–AuNPs showed a similar trend. As illustrated in Figure 1C and Figure 1D, the ECL signal enhanced initially while the concentration of H_2O_2 increased from 0 to 10 mM. Then, the ECL signal weakened with the content of H_2O_2 increasing from 10 to 20 mM. Otherwise, cyclic voltammetry (CV) and the corresponding ECL characterizations were utilized to further explore the ECL process between H_2O_2 and $K_2S_2O_8$. As stated in Figure S4, the reduction current caused by the reduction of H_2O_2 to $OH^\bullet$ was much smaller than that induced by the reduction of $S_2O_8^{2-}$ to $SO_4^{\bullet-}$. Accordingly, compared with the ECL caused by $K_2S_2O_8$ (5684 au), the ECL intensity caused by H_2O_2 (286 au) was very small. However, when combined 10 mM H_2O_2 and 0.1 M $K_2S_2O_8$ together as dual coreactants, the ECL intensity (16832 au) was much stronger than the sum of the ECL signals when 10 mM H_2O_2 and 0.1 M $K_2S_2O_8$ acted as an individual coreactant, respectively. The results illustrated that $SO_4^{\bullet-}$ had a stronger oxidizing capacity for the formation of $C_3N_4^+$ compared with that of $OH^\bullet$. Therefore, the enhanced ECL intensity of the C_3N_4–AuNPs electrode with dual coreactants also arises from the increase of $SO_4^{\bullet-}$ by H_2O_2 on the electrode surface, which has been confirmed on semiconductor TiO_2 nanotubes (NTs) electrode with electron paramagnetic resonance (EPR) technique.[21] Therefore, the possible reactions among C_3N_4, H_2O_2, and $S_2O_8^{2-}$ on GCE are listed as follows:[21,22]

(i) electrochemical reduction

$$S_2O_8^{2-} + e^- \rightarrow SO_4^{2-} + SO_4^{\bullet-} \quad (1)$$

$$H_2O_2 + e^- \rightarrow OH^- + OH^\bullet \quad (2)$$

(ii) synergistic effect

$$SO_4^{\bullet-} + H_2O \rightarrow HSO_4^- + OH^\bullet \quad (3)$$

or

$$OH^\bullet + S_2O_8^{2-} \rightarrow HSO_4^- + SO_4^{\bullet-} + 1/2O_2 \quad (4)$$

(iii) ECL emission

$$SO_4^{\bullet-} \rightarrow SO_4^{2-} + h^+ \quad (6)$$

$$C_3N_4 + h^+ \rightarrow C_3N_4^+ \quad (7)$$

$$C_3N_4^+ + e^- \rightarrow C_3N_4^* \quad (8)$$

$$C_3N_4^* \rightarrow C_3N_4 + h\nu \quad (9)$$

(iv) excessive H_2O_2

$$OH^\bullet + SO_4^{\bullet-} \rightarrow HSO_4^- + 1/2O_2 \quad (10)$$

As discussed above, the ECL enhancement of the C_3N_4 by dual coreactants attributed to the principal effect of $K_2S_2O_8$, the intermediate ($SO_4^{\bullet-}$) of which generated the excited states of C_3N_4. $SO_4^{\bullet-}$ was obtained by electrochemical reduction and decomposition of $S_2O_8^{2-}$ induced by $OH^\bullet$. As the content of $OH^\bullet$ increased, $OH^\bullet$ was converted from promoting the formation of $SO_4^{\bullet-}$ to scavenge the $SO_4^{\bullet-}$. Therefore, with the increase of H_2O_2, the ECL intensity was enhanced initially and then reduced.

The Bidirectional ECL Sensing Principle. In this study, the biosensor was fabricated by assembling DNAzyme-MBs on C_3N_4–AuNPs modified GCE. Then the electrode was immersed into the BCP solution, hemin/G-quadruplex would convert 4-CN into benzo-4-chlorohexadienone in the presence of H_2O_2, and then the precipitate would adhere to the surface of the electrode for further ECL measurement. Therefore, the assembly of hemin/G-quadruplex was considered to be dual functional. One side, the ECL of C_3N_4–AuNPs is inhibited by

DOI: 10.1021/acs.analchem.9b02914
Anal. Chem. 2019, 91, 12000–12005

excessive H_2O_2 (Figure 1). The hemin/G-quadruplex, the same as the horseradish peroxidase, can promote the catalytic reduction of H_2O_2 by the two following steps (eqs 1 and 2).[23,24]

$$\text{hemin/G-quadruplex } (Fe^{III}) + e \rightarrow \text{hemin/G-quadruplex } (Fe^{II}) \quad (11)$$

$$\text{hemin/G-quadruplex } (Fe^{II}) + 1/2H_2O_2 \rightarrow \text{hemin/G-quadruplex } (Fe^{III}) + OH^- \quad (12)$$

Therefore, the repression of the ECL of C_3N_4–AuNPs would be reduced as the H_2O_2 was consumed catalytically. On the other side, DNAzyme-MBs and benzo-4-chlorohexadienone, the product involved by enzyme-stimulated BCP, both would block the $S_2O_8^{2-}$ diffused to the C_3N_4. The influence of these two opposite effects on the ECL signal varied with the concentrations of miRNA-141.

In order to prove the assumption, a lower concentration (10^{-14} M) of miRNA-141 was used in the biosensing system. As displayed in Figure 2A, the ECL intensity was much higher

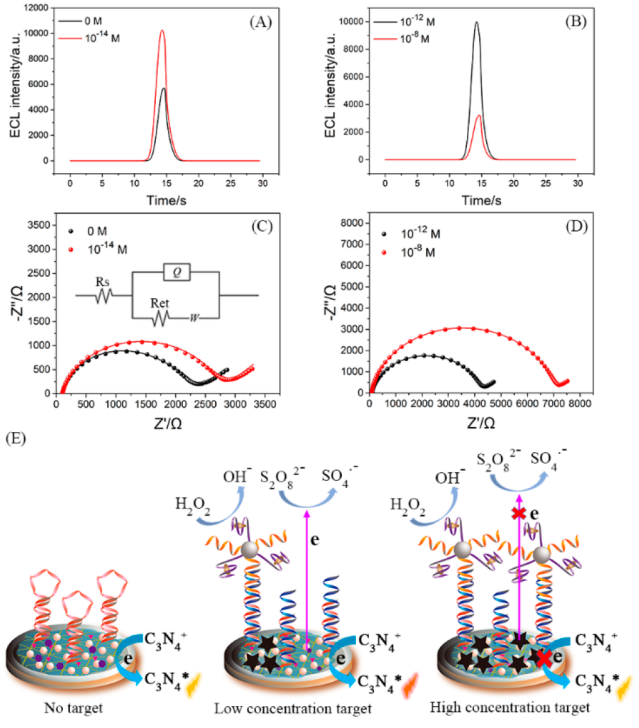

Figure 2. (A, B) ECL responses for reduction of H_2O_2 (20 mM) and (C, D) Nyquist plots (points) and simulations (lines) for the ECL biosensor without or with a low concentration (10^{-14} M) (A, C) and high concentrations (10^{-12} and 10^{-8} M) (B, D) of miRNA-141. (E) Proposed reactions occurring at the ECL biosensor at (left) no, (middle) low, and (right) high concentrations of miRNA-141.

than that without miRNA-141, indicating that the effect of electrocatalytic reduction of H_2O_2 by the hemin/G-quadruplex is predominant. Hence, an obvious recovery of ECL intensity of C_3N_4–AuNPs was obtained. When the concentration of miRNA-141 increased from 1.0 pM to 10 nM, an evident suppression of the ECL intensity of C_3N_4–AuNPs was observed (Figure 2B), indicating a large amount of DNAzyme-MBs and precipitation were formed, leading to evident steric hindrance. This phenomenon could also be proved by EIS data (Figure 2C, 2D). The equivalent circuit observed in Figure 2C was used to fit the EIS data, which includes the solution resistance (Rs), charge transfer resistance (Ret), constant phase element (Q), and Warburg impedance (W). At a lower target concentration, a slight change of the Ret was observed (Figure 2C). The Ret increased from 2156 to 2608 Ω with the increase of the concentration of miRNA-141 from 0 to 10 fM. However, Ret increased remarkably from 4094 to 6877 Ω when the concentration of miRNA-141 increased from 1.0 pM to 10 nM (Figure 2D). To sum up, at a lower concentration of miRNA-141, very few DNAzyme-MBs were assembled on C_3N_4–AuNPs, and the Ret of DNAzyme-MBs and precipitation stimulated by DNAzyme-MBs were small (Figure 2E, middle). On the contrary, large amounts of DNAzyme-MBs and precipitation were formed, leading to evident steric hindrance (Figure 2E, right).

Analytical Performance. Based on the above results, the effective competitive ECL system was applied for sensitive and accurate detection of miRNA-141. As shown in Figure 3A, with the concentration of miRNA-141(in the range of 10^{-17}–10^{-13} M) increase, the ECL intensity of C_3N_4–AuNPs increased gradually. The ECL decreased gradually when the concentration of miRNA-141 further increased from 10^{-13} to 10^{-9} M. Figure 3B shows the relationship between the logarithm of target miRNA-141 concentration and the ECL intensity. At lower concentrations of miRNA-141 ranging from 10^{-17} to 10^{-13} M, the ECL intensity exhibited a favorable positive linear correlation and the correlation coefficient approached 0.995. At higher concentrations of miRNA-141 ranging from 10^{-13} to 10^{-9} M, the ECL intensity showed a good negative linear relationship with a correlation coefficient of 0.996. The limit of detection (LOD) was calculated to be 7.9 aM (S/N = 3), which is much lower than that of the previously reported sensing systems (Table S2). By contrast, we checked the performance of the ECL biosensor without BCP, and the sensor did not show bidirectional sensing property. The ECL intensity displayed a good positive linear relationship with the logarithm of target miRNA-141 concentration changing from 10^{-17} to 10^{-12} M, and then the enhancement of the ECL intensity alleviated while the concentration continued to increase (Figure 3B, hollow circle). This phenomenon illustrated that BCP is the main factor contributing to the steric hindrance effect at higher target concentrations. It also proved by the results of EIS (Figure 3C, 3D). Ret change showed linearity with the logarithm of the miRNA-141concentration between 10 fM and 1.0 nM, and the correlation coefficient reached 0.970 (Figure 3D). In comparison, the Ret exhibited slight change without BCP.

In this bidirectional ECL biosensor, the selectivity was investigated by the comparison of different miRNAs, including single-base mismatched sequence, miRNA-15, miRNA-16, and miRNA-21. Blank was introduced as a reference. As shown in Figure 4, the ECL signal showed a maximum intensity for miRNA-141 (a) compared with others at the concentration of 10^{-14} M (Figure 4A) and 10^{-12} M (Figure 4B), respectively. The ECL intensity for single-base mismatched sequence (b) was slightly stronger compared with others but still much lower than that for miRNA-141 (a). In addition, miRNA-15 (c), miRNA-16 (d), and miRNA-21 (e) represented almost the same ECL intensity as blank (f) in both target concentrations. The results suggested a great selectivity of the proposed ECL biosensor.

DOI: 10.1021/acs.analchem.9b02914
Anal. Chem. 2019, 91, 12000–12005

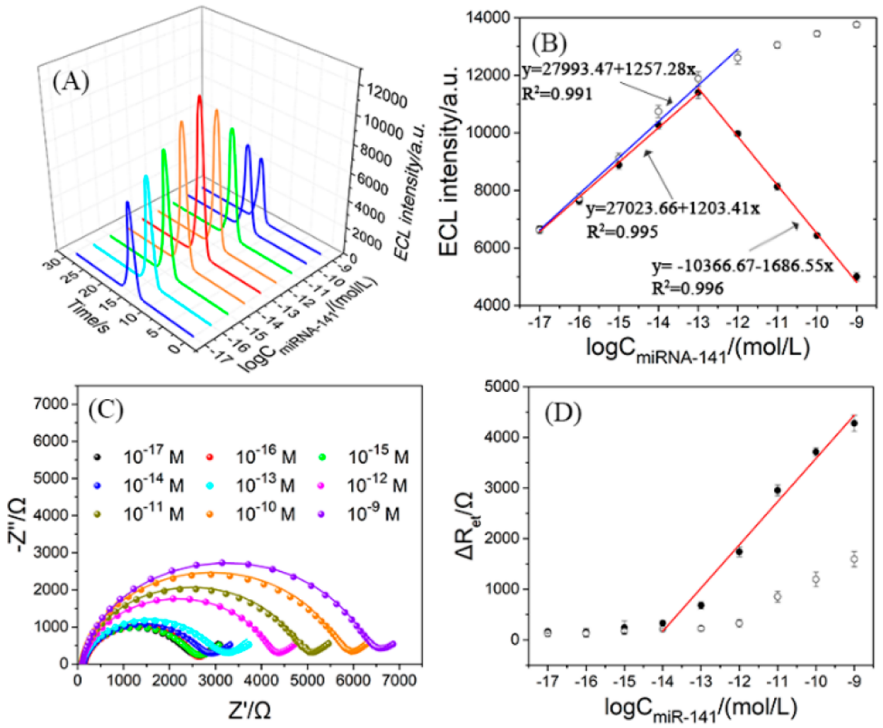

Figure 3. (A) ECL profiles of the ECL biosensor for miRNA-141 with concentrations ranging from 10^{-17} to 10^{-9} M. (B) Calibration curves for miRNA-141 detection by the bidirectional ECL biosensor (solid circle) and the ECL biosensor without BCP (hollow circle). (C) Nyquist plots (points) of the biosensor for miRNA-141 with concentrations ranging from 10^{-17} to 10^{-9} M and simulation (lines). (D) Calibration curves for miRNA-141 detection based on EIS data by the biosensor with (solid circle) and without BCP (hollow circle). Error bars represented the standard deviations for each set of three parallel experiments.

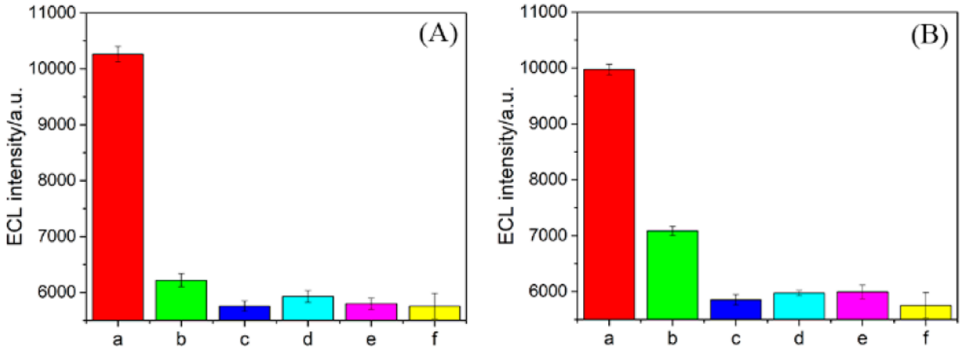

Figure 4. Bar graphs of the bidirectional ECL biosensor for different RNA sequences with 10^{-14} M (A) and 10^{-12} M (B): (a) miRNA-141, single-base mismatched sequence (b), miRNA-15 (c), miR-NA-16 (d), and miRNA-21 (e). Blank (f) was introduced as a reference. The ECL was measured in 0.01 M PBS containing 0.1 M $K_2S_2O_8$ and 20 mM H_2O_2. Error bars represented the standard deviations for each set of three parallel experiments.

Real Sample Analysis. The practical application of the bidirectional ECL biosensor was investigated by determining the concentration of miRNA-141 added to real samples. In consideration that we did not have human serum samples with true values of miRNA-141, we adopted standard addition of miRNA-141 in normal fetal calf serum for practical application. MiRNA-141 solution was injected into 10% diluted normal fetal calf serum. As displayed in Table 1, the results showed great recoveries from 93% to 107% and RSDs from 1.8% to 4.3%, which indicated that the proposed biosensor possesses excellent potential in clinical detection of miRNA-141.

Table 1. Recovery Tests for miRNA-141 in Spiked Fetal Calf Serum Samples (n = 3)

samples	added	found	RSD (%)	recovery (%)
1	10.0 fM	10.6 fM	4.3	106
2	100 fM	97 fM	3.8	97
3	1.00 pM	1.03 pM	3.5	103
4	10.0 pM	9.3 pM	1.8	93
5	100 pM	107 pM	2.0	107

CONCLUSION

In summary, we developed a bidirectional ECL biosensor for miRNA-141 based on the competition between catalysis and

DOI: 10.1021/acs.analchem.9b02914
Anal. Chem. 2019, 91, 12000−12005

steric hindrance. It showed an ultralow detection limit of 7.9 aM and a two-segment linear range with 8 orders of magnitude. Due to the two competitive mechanisms, the detection performance showed evident superiority compared with those of single-mechanism ECL sensors. This biosensing system would provide an important reference for the detection of biomolecules with high sensitivity and wide detection range.

■ ASSOCIATED CONTENT

Supporting Information

The Supporting Information is available free of charge on the ACS Publications website at DOI: 10.1021/acs.analchem.9b02914.

Reagents and apparatus; EIS characterization of miRNA ECL sensing system; characterization of C_3N_4 and C_3N_4-AuNPs; characterization of the C_3N_4-AuNPs modified electrode; stability of the ECL biosensor and comparison with other reported miRNA detection methods (PDF)

■ AUTHOR INFORMATION

Corresponding Authors

*E-mail: weizhao@nju.edu.cn. Tel./Fax: +86-25-89687294.
*E-mail: xujj@nju.edu.cn. Tel./Fax: +86-25-89687294.

ORCID

Wei Zhao: 0000-0002-9526-2008
Jing-Juan Xu: 0000-0001-9579-9318

Author Contributions

The manuscript was written through contributions of all authors. All authors have given approval to the final version of the manuscript.

Notes

The authors declare no competing financial interest.

■ ACKNOWLEDGMENTS

This work was supported by the National Key R&D Program of China (Grant No. 2016YFA0201200) and the National Natural Science Foundation (Grants 21535003) of China. This work was also supported by Excellent Research Program of Nanjing University (ZYJH004).

■ REFERENCES

(1) He, L.; Hannon, G. J. *Nat. Rev. Genet.* **2004**, *5*, 522.
(2) Manikandan, J.; Aarthi, J. J.; Kumar, S. D.; Pushparaj, P. N. *Bioinformation* **2008**, *2*, 330−334.
(3) Hu, T.; Zhang, L.; Wen, W.; Zhang, X.; Wang, S. *Biosens. Bioelectron.* **2016**, *77*, 451−456.
(4) Wu, X.; Chai, Y.; Zhang, P.; Yuan, R. *ACS Appl. Mater. Interfaces* **2015**, *7*, 713−720.
(5) Fang, S.; Lee, H. J.; Wark, A. W.; Corn, R. M. *J. Am. Chem. Soc.* **2006**, *128*, 14044−14046.
(6) Liu, H.; Li, L.; Wang, Q.; Duan, L.; Tang, B. *Anal. Chem.* **2014**, *86*, 5487−5493.
(7) Cheng, Y.; Lei, J.; Chen, Y.; Ju, H. *Biosens. Bioelectron.* **2014**, *51*, 431−436.
(8) Richter, M. M. *Chem. Rev.* **2004**, *104*, 3003−3036.
(9) Jiang, X.; Chai, Y.; Wang, H.; Yuan, R. *Biosens. Bioelectron.* **2014**, *54*, 20−26.
(10) Xie, S.; Dong, Y.; Yuan, Y.; Chai, Y.; Yuan, R. *Anal. Chem.* **2016**, *88*, 5218−5224.
(11) Li, G.; Yu, X.; Liu, D.; Liu, X.; Li, F.; Cui, H. *Anal. Chem.* **2015**, *87*, 10976−10981.
(12) Cui, C.; Chen, Y.; Jiang, D.; Zhu, J.-J.; Chen, H.-Y. *Anal. Chem.* **2017**, *89*, 2418−2423.
(13) Xu, J.; Zhang, Y.; Li, L.; Kong, Q.; Zhang, L.; Ge, S.; Yu, J. *ACS Appl. Mater. Interfaces* **2018**, *10*, 3431−3440.
(14) Wu, L.; Ding, F.; Yin, W.; Ma, J.; Wang, B.; Nie, A.; Han, H. *Anal. Chem.* **2017**, *89*, 7578−7585.
(15) Lv, Y.; Chen, S.; Shen, Y.; Ji, J.; Zhou, Q.; Liu, S.; Zhang, Y. *J. Am. Chem. Soc.* **2018**, *140*, 2801−2804.
(16) Cheng, C.; Huang, Y.; Tian, X.; Zheng, B.; Li, Y.; Yuan, H.; Xiao, D.; Xie, S.; Choi, M. M. F. *Anal. Chem.* **2012**, *84*, 4754−4759.
(17) Feng, Q.-M.; Shen, Y.-Z.; Li, M.-X.; Zhang, Z.-L.; Zhao, W.; Xu, J.-J.; Chen, H.-Y. *Anal. Chem.* **2016**, *88*, 937−944.
(18) Chen, L.; Zeng, X.; Si, P.; Chen, Y.; Chi, Y.; Kim, D.-H.; Chen, G. *Anal. Chem.* **2014**, *86*, 4188−4195.
(19) Wang, Y. Z.; Zhao, W.; Dai, P. P.; Lu, H. J.; Xu, J. J.; Pan, J.; Chen, H. Y. *Biosens. Bioelectron.* **2016**, *86*, 683−689.
(20) Datta, K. K. R.; Reddy, B. V. S.; Ariga, K.; Vinu, A. *Angew. Chem., Int. Ed.* **2010**, *49*, 5961−5965.
(21) Dai, P.-P.; Yu, T.; Shi, H.-W.; Xu, J.-J.; Chen, H. Y. *Anal. Chem.* **2015**, *87*, 12372−12379.
(22) Choi, J. P.; Bard, A. J. *Anal. Chim. Acta* **2005**, *541*, 143−150.
(23) Zhou, H.; Zhang, Y.-Y.; Liu, J.; Xu, J. J.; Chen, H. Y. *Chem. Commun.* **2013**, *49*, 2246−2248.
(24) Deng, S.; Cheng, L.; Lei, J.; Cheng, Y.; Huang, Y.; Ju, H. *Nanoscale* **2013**, *5*, 5435−5441.

DOI: 10.1021/acs.analchem.9b02914
Anal. Chem. 2019, 91, 12000−12005